Noise-induced dephasing in neutron interferometry

G. Sulyok,[1] Y. Hasegawa,[1] J. Klepp,[2] H. Lemmel,[1,3] and H. Rauch[1]
[1]*Atominstitut, Technische Universität Wien, 1020 Vienna, Austria*
[2]*Faculty of Physics, University of Vienna, 1090 Vienna, Austria*
[3]*Institut Laue-Langevin, F-38042 Grenoble, France*
(Received 26 February 2010; published 11 May 2010)

Decoherence phenomenona in a neutron interferometer are analyzed by simulation of the effects of an environment with magnetic noise fields. Basic calculations and experiments show the validity and limitations of this model system. In particular, loss and recovery of the interference pattern with controllable noise sources in both interferometer arms are discussed in detail. In addition, the decoherence behavior at high interference order, where Schrödinger-cat-like states exist in the interferometer, is investigated. While at low interference order a smearing of the interference pattern is observed, at high interference order a smearing of the modulated momentum distribution occurs.

DOI: 10.1103/PhysRevA.81.053609 PACS number(s): 03.75.Dg, 03.65.Yz, 42.50.−p

I. INTRODUCTION

Interferometers of different types have become standard tools for the demonstration of wave properties of massive particles, underlining the validity of quantum mechanics for particles like electrons [1,2] or neutrons [3], and even for atoms and molecules with high mass numbers [4,5]. Apart from imperfections of the whole interferometer setup, observation of interference properties is complicated because of decoherence effects caused by the environment. The theory of open quantum systems [6–9] provides explanations for the associated loss of coherence. The interaction between the observed system and the environment causes their entanglement and destroys the unitary evolution of the system and its quantum behavior. Experimental observations of decoherence processes have been reported, for example, with electrons coupling to an electron gas inside a semiconducting plate [10], with molecules colliding with background gases [11], and with molecules decohering by thermal emission of radiation [12]. A profound understanding of these decoherence phenomena also leads to a deeper understanding of the transition between the quantum regime and the classical world. In this context, Stern *et al.* [13] have proved that the loss of coherence can also be described by statistically distributed phase accumulations of the interfering waves.

In the case of neutrons, these phases can be caused by the magnetic dipole interaction described by the Zeeman-Hamiltonian $\hat{H} = -\mu\vec{\sigma}\cdot\vec{B}$. During their flight through the field region, the neutrons accumulate a phase given by $\phi = (\mu/\hbar)\vec{\sigma}\cdot\int\vec{B}dt$. In our experiments, the phase derives from a classical noise field that is time dependent and causes energy exchange in the form of photon absorption or emission, as calculated and measured by Summhammer and co-workers [14,15]. Since the states of the magnetic field do not change in the photon exchange process, there is no entanglement between the neutron and the field, but the effects of the statistically distributed phase shifts on the observed interference pattern are equivalent to the effects of a quantum-mechanical environment [13]. For a more detailed description of the connection between noise fields and decoherence effects in the framework of Lindblad master equations, see [16].

We investigate the dephasing effect as a function of the strength of the Gaussian noise field, which shows the response to the dynamical quantum phase. The geometrical phase remains unchanged since the field acts along the same direction and no area is enclosed owing to the excursion in parameter space. A study of the stability of the geometrical phase and its contribution to the dephasing process has been published recently [17].

Another prediction of decoherence theory concerns macroscopically distinguishable states (so-called Schrödinger-cat-like states) whose sensitivity to external fluctuations increases when their spatial separation increases [8,18]. In the neutron interferometer, these states can be produced by thick phase shifters, when the phase shifts become larger than the coherence lengths [19,20].

The work presented is organized as follows. In Sec. II, basic formulas are developed for calculating the interferometer contrast when magnetic noise fields are applied in the interferometer. Section III A focuses on the experimental results for the standard interferometric setup (phase contrast measurements). Contrast behavior for a noise field with different frequency bandwidths is investigated. Further, for noise fields applied in each interferometer arm, both the cases of correlated and uncorrelated signals are discussed. In Sec. III B, the preparation of Schrödinger-cat-like states in the neutron interferometer and their properties are explained. These states are then exposed to magnetic noise and the effect on the arising momentum modulation is examined.

II. THEORY

Before addressing the actual experiments, we briefly review the connection between the measured interferometer contrast and the neutron state. Following the density-matrix approach [21], we write the incoming state as

$$\rho_{\text{in}} = |0\rangle\langle 0| \otimes \rho_{\text{spin}} = \begin{pmatrix} 1 & 0 \\ 0 & 0 \end{pmatrix} \otimes \rho_{\text{spin}}. \tag{1}$$

For the path degree of freedom, there are only two possible states, namely, $|0\rangle$ (denoting the direction of the incoming O beam) and $|1\rangle$ (denoting the direction of the reflected

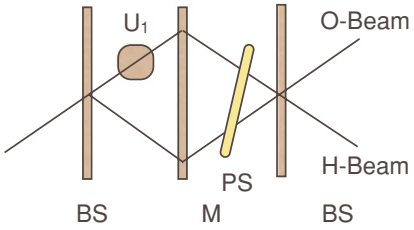

FIG. 1. (Color online) Schematic setup for the interferometer (IFM) with a unitary operation in one beam path.

H beam). The action of the whole interferometer setup (see Fig. 1) combines the beam splitters (BSs), the unitary transformation (U) acting only on the spin part of the wave function, the phase shifter (PS), and the mirror (M), yielding, for the output state,

$$\rho_{\text{out}} = U_{\text{BS}} U_{\text{PS}} U_{\text{M}} U U_{\text{BS}}\ \rho_{\text{in}}\ U_{\text{BS}}^{\dagger} U^{\dagger} U_{\text{M}}^{\dagger} U_{\text{PS}}^{\dagger} U_{\text{BS}}^{\dagger}, \tag{2}$$

with

$$U_{\text{BS}} = \frac{1}{\sqrt{2}} \begin{pmatrix} 1 & i \\ i & 1 \end{pmatrix} \otimes \mathbb{1}, \quad U_{\text{M}} = \begin{pmatrix} 0 & 1 \\ 1 & 0 \end{pmatrix} \otimes \mathbb{1},$$
$$U_{\text{PS}} = \begin{pmatrix} e^{i\chi} & 0 \\ 0 & 1 \end{pmatrix} \otimes \mathbb{1}, \tag{3}$$
$$U = \begin{pmatrix} 1 & 0 \\ 0 & 0 \end{pmatrix} \otimes U_1 + \begin{pmatrix} 0 & 0 \\ 0 & 1 \end{pmatrix} \otimes \mathbb{1}.$$

The intensity in the O direction is given by

$$I_{\text{O}} = \text{tr}(P_{\text{meas}} \rho_{\text{out}}) = \text{tr}\left[\begin{pmatrix} 1 & 0 \\ 0 & 0 \end{pmatrix} \otimes \mathbb{1} \cdot \rho_{\text{out}} \right]$$
$$= \frac{1}{2}[1 + a\cos(\chi - \xi)], \tag{4}$$

where $ae^{i\xi} = \text{tr}(U_1 \rho_{\text{spin}}) = |\text{tr}(U_1 \rho_{\text{spin}})| e^{i \arg \text{tr}(U_1 \rho_{\text{spin}})}$. The amplitude a of the oscillation corresponds to the interferometer contrast.

Tracing over the spin degree of freedom of ρ_{out} yields

$$\rho_{\text{path}} = \frac{1}{2} \begin{pmatrix} 1 + a\cos(\chi - \xi) & -a\sin(\chi - \xi) \\ -a\sin(\chi - \xi) & 1 - a\cos(\chi - \xi) \end{pmatrix}, \tag{5}$$

showing explicitly that a vanishing contrast ($a \to 0$) indicates a totally mixed path density matrix. For a purely time-dependent magnetic field pointing in a fixed direction $\vec{n}_B$, the transformation U_1 on the incoming neutron is [22]

$$U_1 = \exp\left(-i \frac{\mu}{\hbar} \vec{\sigma} \cdot \vec{n}_B \int_{t_i}^{t_i + T} B(t) dt \right), \tag{6}$$

where $T = l/v$ denotes the time of flight of the neutron through the field region, l is the length of the field region, and v is the group velocity of the neutron. The neutron enters the field region at t_i. If the time of flight through the magnetic field is considerable shorter than the typical time variation of the field, one can use the quasistatic approximation and replace Eq. (6) by

$$U_1 = \exp\left(-i \frac{\mu}{\hbar} \vec{\sigma} \cdot \vec{n}_B\ T B(t_i) \right). \tag{7}$$

For unpolarized neutrons one obtains

$$\text{tr}(U_1 \rho_{\text{spin}}) = \cos\left(\frac{\mu}{\hbar} \frac{l}{v} B(t_i) \right). \tag{8}$$

The phase shift $\phi = \mu B l / \hbar v$ is directly proportional to the strength of the magnetic field but weakly dependent on small changes of the velocity caused by energy exchange with the time-dependent field. For example, if the frequency band of $B(t)$ ranges from 0 to ω, an exchange of n photons with the mode of highest energy is given by $\Delta E_{n\ \text{photons}} = \pm n\hbar\omega$. For an upper frequency of about 100 kHz, the relative change of the velocity amounts to only $\Delta v_{n\ \text{photons}}/v \simeq \Delta E_{n\ \text{photons}}/2E_{\text{kin}} \simeq n \times 10^{-8}$. Thus, it can be neglected compared to the velocity distribution of the incoming beam, $\Delta v/v = \Delta\lambda/\lambda \simeq 10^{-2}$.

The experimentally measured contrast C results from summation over all entrance times,

$$C = \sum_i \cos\left(\frac{\mu}{\hbar} \frac{l}{v} B(t_i) \right) \simeq \frac{1}{T_m} \int_0^{T_m} \cos\left(\frac{\mu}{\hbar} \frac{l}{v} B(t) \right) dt, \tag{9}$$

where T_m denotes the measurement time. The time integral can be replaced by an integral over the distribution of the field amplitudes,

$$C = \int_{-\infty}^{+\infty} P(B) \cos\left(\frac{\mu}{\hbar} \frac{l}{v} B \right) dB. \tag{10}$$

A single neutron travels through a region with a constant magnetic field but the whole neutron ensemble experiences the amplitude distribution $P(B)$ of the field.

If transformations are applied in both beam parts, an analogous calculation where

$$U = \begin{pmatrix} 1 & 0 \\ 0 & 0 \end{pmatrix} \otimes U_1 + \begin{pmatrix} 0 & 0 \\ 0 & 1 \end{pmatrix} \otimes U_2 \tag{11}$$

yields for the intensity in the O beam

$$I_{\text{O}} = \text{Tr}(P_{\text{meas}} \rho_{\text{out}}) = \tfrac{1}{2}\{[1 + b\cos(\chi - \xi)]\} \tag{12}$$

with $be^{i\xi} = \text{Tr}(U_2^{\dagger} U_1 \rho_{\text{spin}})$. For two time-dependent magnetic fields, the expression $U_2^{\dagger} U_1$ has the form

$$U_2^{\dagger} U_1 = \exp\left\{ i \frac{\mu}{\hbar} \vec{\sigma} \cdot \int_{t_i}^{t_i + T} \left[\vec{B}_2\left(t - \frac{\Delta x}{v} \right) - \vec{B}_1(t) \right] dt \right\}, \tag{13}$$

where $\Delta x = x_1 - x_2$ denotes the difference between the lengths of the two beam paths from the first interferometer plate to the position where the transformation U_i takes places (e.g., the position of the coils). The resulting contrast for unpolarized neutrons and quasistatic fields is given by

$$C = \frac{1}{T_m} \int_0^{T_m} \cos\left\{ \frac{\mu}{\hbar} \frac{l}{v} \left[B_2\left(t - \frac{\Delta x}{v} \right) - B_1(t) \right] \right\} dt. \tag{14}$$

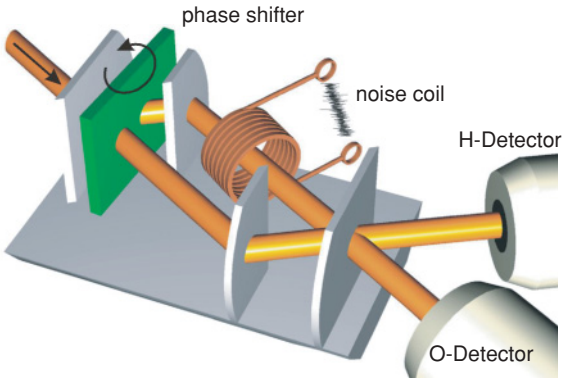

FIG. 2. (Color online) Setup for experiments in position space (phase shifts are smaller than the coherence length, and the intensity oscillates between the two detectors).

III. EXPERIMENTAL RESULTS

A. Phase contrast measurements

All experiments described here have been performed at the S18 neutron interferometry setup at the high-flux reactor of the Institute Laue-Langevin in Grenoble, France. A silicon perfect-crystal monochromator is placed behind a neutron guide to extract neutrons of mean wavelength $\lambda = 1.92$Å ($\delta\lambda/\lambda \simeq 0.01$) and a beam cross section of 6×8 mm^2. The unpolarized neutrons impinge on the skew-symmetric silicon interferometer at an angle of 30°. Therefore, the Bragg condition is satisfied for the 220 lattice planes and the interferometer plates act as described in Sec. II. The schematic setup is depicted in Fig. 2. We now apply Gaussian white magnetic noise in one interferometer arm with the field pointing in beam direction (preliminary results of such measurements have been published elsewhere [23,24]). The field is generated by a fluctuating current in a coil connected to a Tektronix random signal generator AFG 3022b. The length l of the effective field region is 42.65 mm, leading to a time of flight of about 20.7 μs. The characteristics of the input signal are shown in Fig. 3. If the dynamics of the noise field is properly adjusted, that is, the quasistatic approximation is valid, the formula for the interferometer contrast is given by [see Eq. (10)]

$$C = \int_{-\infty}^{+\infty} \frac{1}{\sqrt{2\pi}\,\Delta B} e^{-B^2/2(\Delta B)^2} \cos\left(\frac{\mu}{\hbar}\frac{l}{v}B\right) dB$$
$$= \exp\left[-\frac{1}{2}\left(\frac{\mu l}{\hbar v}\Delta B\right)^2\right] \equiv \exp\left(-\frac{1}{2}(\Delta\phi)^2\right), \qquad (15)$$

where $\Delta\phi$ denotes the standard deviation of the phase fluctuations related to the standard deviation ΔB of the noise field. In order to compensate loss of contrast that is not due to the magnetic noise field (mainly induced by temperature fluctuations and vibrations), on-off contrast measurements have been performed. For each position of the phase shifter, the intensity is measured with and without noise. The contrasts of the resulting oscillations are determined [$C = (I_{\max} - I_{\min})/(I_{\max} + I_{\min})$], and their quotient gives the relative contrast (see Fig. 4). The interferograms are always

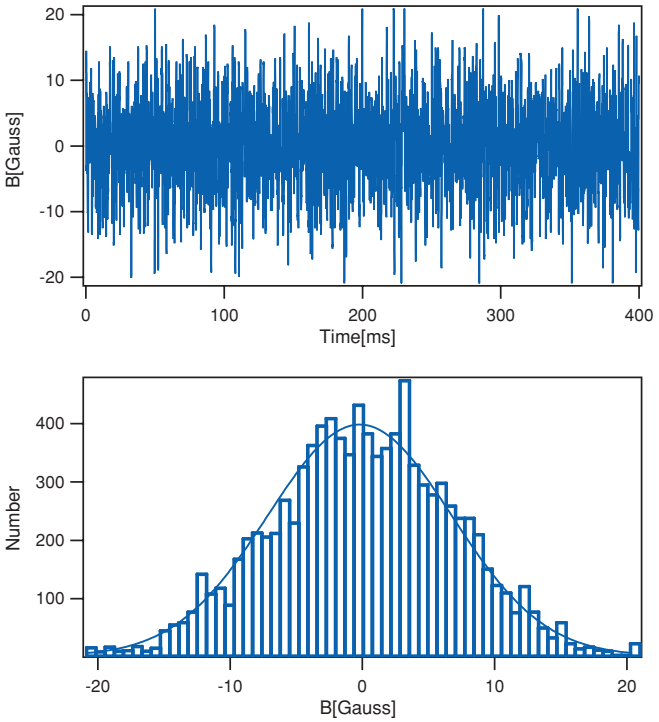

FIG. 3. (Color online) Typical Gaussian noise signal and its corresponding histogram.

plotted against the path difference ΔD of the two neutron beams through the phase shifter. This (optical) path difference causes a phase shift $\chi = -Nb_c\lambda\Delta D$ between the two beams, where N denotes the atom density, b_c the coherent scattering length, and λ the neutron wavelength.

For the quasistatic regime (frequency bandwidth $\Delta f =$ 0–5 kHz), experimental data verify the $\exp[-(\Delta\phi)^2/2]$ dependence of the contrast with high accuracy (see Fig. 5).

Thus, it can be concluded that a sufficiently strong noise field leads to a dephased behavior for the whole neutron ensemble. After the third interferometer plate, the averaged path density matrix then looks like a classical mixture

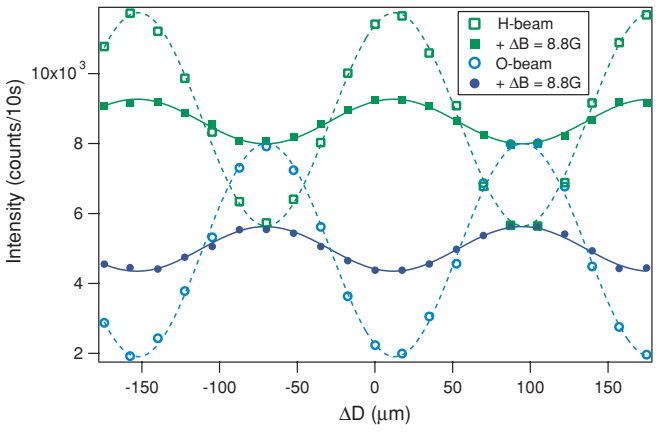

FIG. 4. (Color online) Characteristic interference pattern for noise on-off measurement. Oscillations are damped by the fluctuating field. Error bars are of comparable size to the markers and have been omitted.

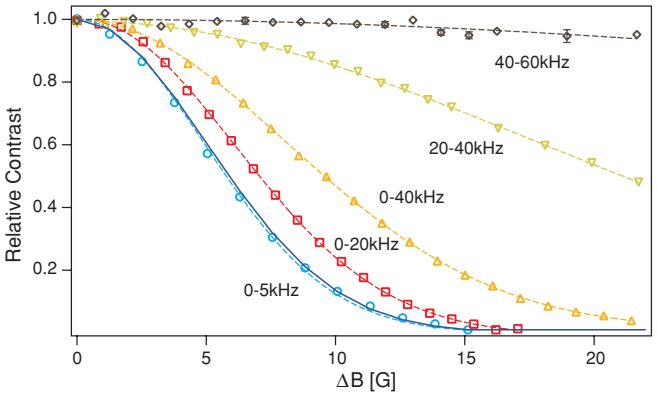

FIG. 5. (Color online) Loss of contrast as a function of the standard deviation of the Gaussian-distributed field amplitudes caused by magnetic noise with different frequency bandwidths Δf. The dashed lines are exponential fits whereas the solid line represents the theory curve in the quasistatic regime. Error bars of comparable size to the markers have been omitted.

since the intensity no longer oscillates between the O and H detectors:

$$\rho_{\text{path}} = \frac{1}{2}\begin{pmatrix} 1+e^{-(\Delta\phi)^2/2}\cos\chi & -e^{-(\Delta\phi)^2/2}\sin\chi \\ -e^{-(\Delta\phi)^2/2}\sin\chi & 1-e^{-(\Delta\phi)^2/2}\cos\chi \end{pmatrix} \rightarrow \frac{1}{2}\begin{pmatrix} 1 & 0 \\ 0 & 1 \end{pmatrix}. \quad (16)$$

Note that this (nonunitary) evolution of the neutron path state is an effective realization of a Lindblad master equation [25] with a single dissipator term Γ,

$$\dot{\rho} = -\frac{i}{\hbar}[H,\rho] + \Gamma^\dagger\rho\Gamma - \frac{1}{2}(\Gamma^\dagger\Gamma\rho + \rho\Gamma^\dagger\Gamma). \quad (17)$$

Now we choose the Hamiltonian to be $H = (\alpha/2)\sigma_y$ and the Lindblad operator to be $\Gamma = \sqrt{\lambda/2}\sigma_y$ acting on the system for a time τ. For the initial state $\rho(0) = |0\rangle\langle 0|$, one obtains in the $(|0\rangle,|1\rangle)$ basis (the eigenstates of σ_z)

$$\rho(\tau) = \frac{1}{2}\begin{pmatrix} 1+e^{-\lambda\tau}\cos\alpha\tau & -e^{-\lambda\tau}\sin\alpha\tau \\ -e^{-\lambda\tau}\sin\alpha\tau & 1-e^{-\lambda\tau}\cos\alpha\tau \end{pmatrix}. \quad (18)$$

If we identify the rotation angle $\alpha\tau$ with the angle χ and the damping factor $\lambda\tau$ with $(\Delta\phi)^2/2$, the correspondence of Eqs. (16) and (17) is clearly visible. A similar approach can be found in [16].

If the frequency bandwidth of the noise signal is enlarged, the quasistatic approximation is no longer valid, and the exponential decay is weakened, $C = \exp[-\gamma(\Delta\phi)^2/2]$, described by a fit parameter $\gamma < 1$ (see Fig. 5). A detailed analysis of the frequency dependence of $\gamma = \gamma(\Delta f)$ will be treated in a forthcoming presentation.

It should be kept in mind that, in a time-resolved measurement, the interference pattern could, in principle, be restored. The loss of contrast can also be reversed when the same noise signal is applied in the second beam path. This can be achieved with an identical second coil driven by the same current (see Fig. 6). If the positions of the two coils in the interferometer are not symmetric, an additional time delay Δt has to be implemented to compensate for the position difference Δx. Equation (14) then becomes [$\phi_i = (\mu/\hbar)(l/v)B_i$]

$$C = \frac{1}{T_m}\int_0^{T_m}\cos\left[\phi_2\left(t+\Delta t-\frac{\Delta x}{v}\right)-\phi_1(t)\right]dt. \quad (19)$$

For identical, synchronized noise signals ($\phi_1 = \phi_2 = \phi$ and $\Delta t = \Delta x/v$), recovery of full contrast can be achieved ($C = 1$) and has been experimentally verified (see Fig. 7).

For identical, unsynchronized noise, or two completely different noise signals, the dephasing process is enforced. For different signals with the same frequency bandwidth Δf, the $e^{-\gamma(\Delta\phi_i)^2/2}$ factors of the two Gaussian noise fields contribute multiplicatively to the contrast (see Fig. 8),

$$C = \exp\left(-\tfrac{1}{2}\gamma[(\Delta\phi_1)^2+(\Delta\phi_2)^2]\right). \quad (20)$$

In the quasistatic case ($\gamma = 1$), this formula results from averaging over an uncorrelated two-dimensional Gaussian distribution for B_1 and B_2 with mean values $B_1^0 = B_2^0 = 0$, correlation coefficient $\sigma_{12} = 0$, and standard deviations ΔB_1

FIG. 6. (Color online) Experimental setup with two coils.

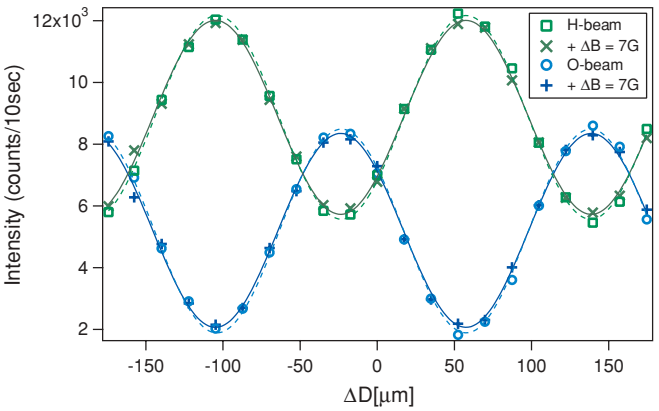

FIG. 7. (Color online) Interferogram for identical synchronized noise in both arms. Contrast remains when noise is turned on.

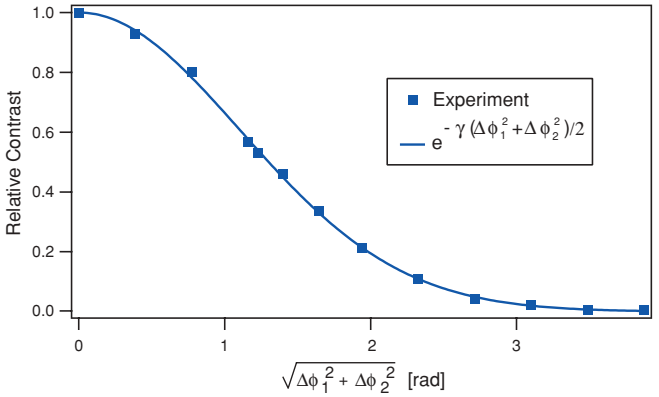

FIG. 8. (Color online) Contrast for independent noise sources in the coils plotted against $\sqrt{\Delta\phi_1^2+\Delta\phi_2^2}$.

and ΔB_2:

$$C=\int\int P(B_1,B_2)\cos\left(\frac{\mu}{\hbar}\frac{l}{v}(B_2-B_1)\right)dB_1dB_2, \quad (21)$$

where

$$P(B_1,B_2)=N\exp\left\{-\beta\left[\left(\frac{B_1}{\Delta B_1}\right)^2-2\sigma_{12}\left(\frac{B_1}{\Delta B_1}\right)\left(\frac{B_2}{\Delta B_2}\right)+\left(\frac{B_2}{\Delta B_2}\right)^2\right]\right\} \quad (22)$$

with

$$N=\frac{1}{2\pi\Delta B_1\Delta B_2\sqrt{1-\sigma_{12}^2}},\quad \beta=\frac{1}{2\sqrt{1-\sigma_{12}^2}}.$$

For fully correlated noise signals ($\sigma_{12}\to 1$) $\int P(B_1,B_2)dB_2\to\delta(B_1-B_2)$ follows, and Eq. (21) reproduces the result of Eq. (19) for the synchronized case.

If identical noise signals are applied, one can determine the relative positions of the coils in the interferometer by scanning through different time delays and measuring the contrast. Maximum recovery of contrast is achieved when the time delay equals the ratio of the position difference and the neutron velocity $\Delta x/v$. If the coils are shifted relative to each other, the maximum is shifted as well (see Fig. 9).

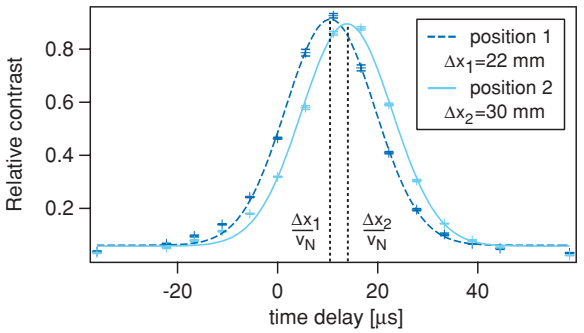

FIG. 9. (Color online) Contrast for the same noise in the two coils but different relative positions Δx_i plotted as a function of the time delay in one coil.

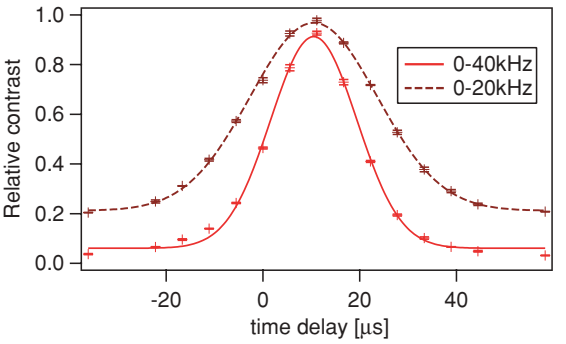

FIG. 10. (Color online) The two coils in the interferometer are driven with the same noise signal. The contrast is plotted for different frequency bandwidths against the time delay in one coil.

The contrast is determined by the cosine of the difference of the two phase shifts in each beam path [see Eq. (19)]. Expansion of the cosine near $\Delta t=\Delta x/v$ reveals the autocorrelation function of the noise signal. If the signal is shifted further, higher terms in the cosine expansion have to be considered, and higher-order autocorrelation terms occur as well. Use of a broader frequency bandwidth for the incoming noise signal narrows the autocorrelation function (see Fig. 10). For ideal white noise it would become a Dirac delta function $\delta(t-\Delta x/v)$.

Because of the interaction of the neutron with a time-dependent field, an energy transfer takes place. For monochromatic noise sources, this energy exchange has already been measured [14] and explained in detail with multiphoton exchange processes [15]. It can be supposed that the concepts used there can be extended for noise signals containing whole frequency bands. The possibility of describing the action of such time-dependent fields in the framework of generalized master equations that explicitly contain dissipative terms will be the subject of further theoretical work as well, but for the time being we use the noise field as an effectively dephasing and easily controllable environment.

B. Momentum modulation measurements

The magnetic noise field is used here to investigate the dephasing of macroscopically distinguishable states, in particular, whether their increasing spatial separation increases their sensitivity to external disturbances [6,8,18]. Schrödinger-cat-like states can be produced in the interferometer with thick aluminum phase shifters that shift the wave packets further than their coherence lengths (on the order of 10 Å) [19,20,23]. The two wave packets traveling through the IFM are separated by a distance $\Delta_x=Nb_c\lambda^2D/2\pi$, where N denotes the atom density, b_c the coherent scattering length of aluminum, D the phase-shifter thickness, and λ the neutron wavelength. The separation width amounts to several 100 Å so that there is essentially no overlap in position space at the third IFM plate any longer. Nevertheless, the wave packets are still in a quantum superposition state described by

$$\psi_{\rm sup}(x,t)=\psi_{\rm I}(x,t)+\psi_{\rm II}(x,t)=\psi_0(x,t)+\psi_0(x+\Delta_x,t), \quad (23)$$

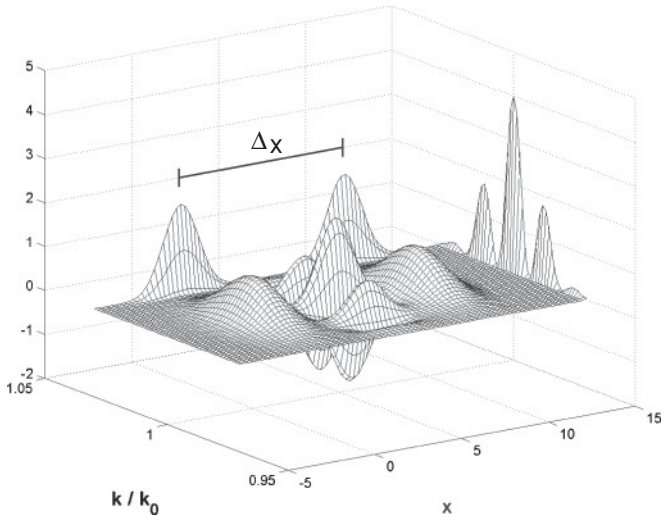

FIG. 11. Wigner function for the macroscopically separated catlike state (x in arbitrary units).

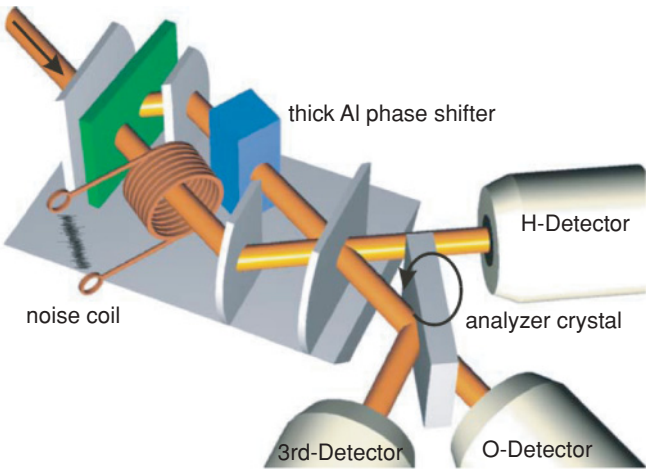

FIG. 12. (Color online) Schematic setup for interference measurements in momentum space with aluminum phase shifter; the intensity oscillates in the wavelength spectrum.

where ψ_{I} and ψ_{II} denote the wave packets arriving from beam paths I and II, respectively. As a good approximation, they have the same form ψ_0; the aluminum slab only shifts the whole wave packet. Thus, both have the same Fourier spectrum $\alpha_0(k)$. The interference properties are exhibited in momentum space,

$$\alpha_{\mathrm{sup}}(k) = \alpha_0(k) + e^{ik\Delta_x}\alpha_0(k),$$
$$|\alpha_{\mathrm{sup}}(k)|^2 = |\alpha_0(k)|^2[1+\cos(k\Delta_x)]. \tag{24}$$

In the Wigner-function representation [26,27]

$$W_{\mathrm{sup}}(x,k) = \frac{1}{2\pi\hbar}\int_{-\infty}^{+\infty} \psi^{\dagger}\left(x+\frac{y}{2}\right)\psi\left(x-\frac{y}{2}\right)e^{iky}dy, \tag{25}$$

both spatial separation and intensity modulation in momentum space are clearly visible (see Fig. 11).

We now expose this Schrödinger-cat-like state to a magnetic noise in one arm of the interferometer, causing a field-dependent phase shift,

$$\psi_{\mathrm{sup}}(B,x,t) = e^{i\phi(B)}\psi_0(x,t) + \psi_0(x+\Delta_x,t). \tag{26}$$

In the quasistatic regime we can evaluate the resulting Wigner function by averaging over the Gaussian distribution of the noise field,

$$\bar{W}(B,x,k,t) = \int_{-\infty}^{+\infty} P(B)W_{\mathrm{sup}}(B,x,k,t)dB, \tag{27}$$

which effects a smearing of the central wiggle structure of the Wigner function, leaving the separated wave packets nearly unchanged. Integration over x yields the probability distribution in momentum space,

$$|\alpha_{\mathrm{sup}}(k)|^2 = |\alpha_0(k)|^2\left[1+e^{-(\mu l^2/\hbar v)(\Delta B)^2/2}\cos(\Delta_x k)\right]. \tag{28}$$

The spatial separation Δ_x does not enter the expression for the contrast, but only the standard deviation ΔB of the magnetic noise field. The loss of contrast is not affected by the separation width of the two Gaussian wave packets. In the experimental setup, we prepared three different Schrödinger-cat-like states by using three different aluminum phase shifters with thicknesses of 18, 27, and 36 mm, which caused packet separations of 212, 318, and 424 Å. To access k space, a silicon analyzer crystal that selects wavelengths via Bragg reflection and a third detector were used (see Fig. 12).

First we determined the wavelength distribution $|\alpha_0(\lambda)|^2$ for the empty interferometer [Fig. 13(a)]. The measured intensity is normalized by the total number of counts in the O beam (the O detector and the third detector). Then

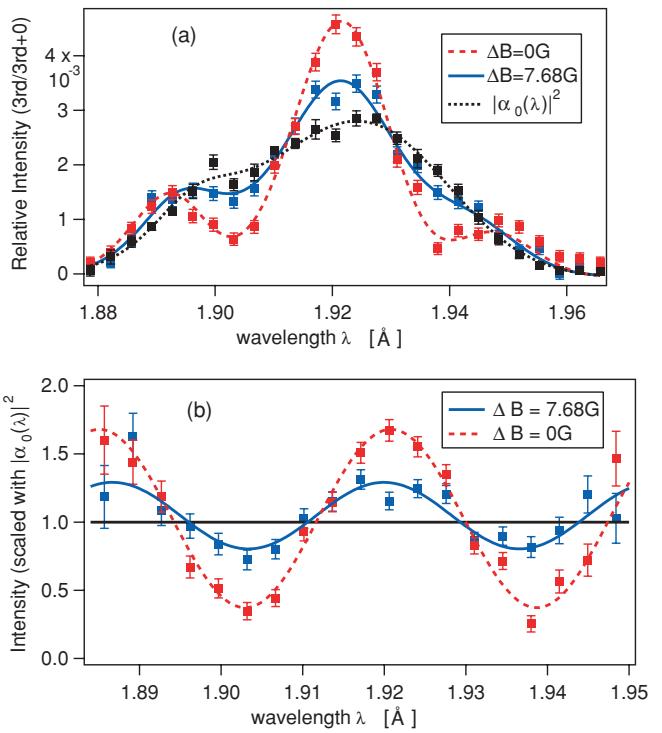

FIG. 13. (Color online) Interferogram in momentum space, wavelength distribution $|\alpha_0(\lambda)|^2$ of the empty interferometer, and original on-off wavelength spectra for $\Delta_x = 212$ Å (a) and on-off curves divided by $|\alpha_0(\lambda)|^2$ (b).

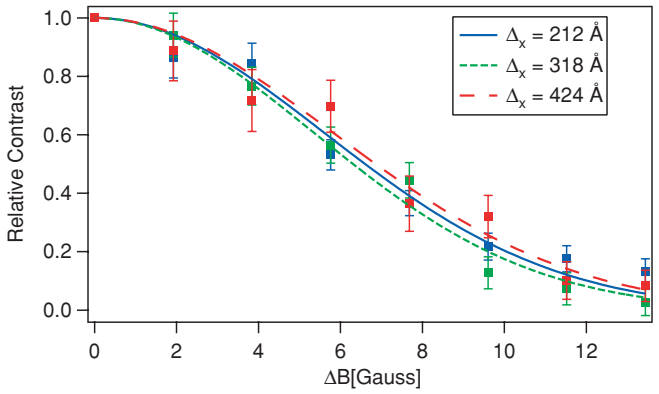

FIG. 14. (Color online) Decoherence behavior for Schrödinger-cat-like states with different separation widths as a function of the strength of the magnetic noise field (exponentially fitted).

the Al phase shifter was inserted, causing a modulation of that spectrum [the curve for $\Delta B = 0$ in Fig. 13(a)]. Turning on the magnetic noise leads to damped modulations. By dividing the modulated spectra by $|\alpha_0(\lambda)|^2$, one gets standard interferograms in cosine form whose contrast can be determined easily [see Fig. 13(b)].

The relative contrast was measured for increasing field strength ($\Delta B = 0$–15 G) and different separation widths (see Fig. 14).

As in Sec. III A, we can neglect the energy transfer between the magnetic field and the neutron because it lies several orders of magnitude below the length of the modulation period. The modulation period is given by the ratio of the wavelength λ and the interference order $n = \Delta_x/\lambda$. It amounts to $\lambda/n \simeq 10^{-2}$ Å, whereas a shift of the wavelength corresponding to the exchange of a 100 kHz photon amounts to $\Delta\lambda \simeq \frac{1}{2}(\hbar\omega/E_{\mathrm{kin}})\lambda \simeq 10^{-8}$ Å. Thus, the modulation pattern is essentially not influenced by the altered neutron velocities. This is the reason that, within measurement accuracy, the separation width has no influence on the relative contrast reduction.

Differences with the results of, for example [8], arise from the different interaction Hamiltonians. In [8], a dipole interaction of the form $\hat{H}_{\mathrm{int}} = \epsilon\hat{x}d\phi(t)/dt$ is assumed that contains the position operator $\hat{x}$ explicitly. This leads to stronger decoherence for increasing spatial separation Δ_x of the Gaussian wave packets. In our case, the interaction between neutron and field is given by $\hat{H}_{\mathrm{int}} = -\mu\vec{\sigma}\cdot\vec{B}$ and "happens" in spin space. Under the quasistatic approximation and negligible energy transfer, only the strength of the field fluctuation ΔB occurs in the expression for the contrast.

In agreement with [28], one can show that the coherent preparation of macroscopically distinct Schrödinger-cat-like states becomes more and more difficult with increasing separation width. The values of the off contrast decrease (see Table I) because of the inhomogeneities of the phase shifters. But this concerns only the preparation of the state, it is not a statement about its stability in principle. As shown in Fig. 14, the loss of contrast because of magnetic noise is the same for each separation width.

TABLE I. Decrease of off-contrast values for thick phase shifters.

Phase shift	$\Delta_x = 212$ Å	$\Delta_x = 318$ Å	$\Delta_x = 424$ Å
Off contrast	$(60.0 \pm 1.1)\%$	$(55.4 \pm 1.1)\%$	$(44.4 \pm 1.3)\%$

IV. CONCLUSION

A magnetic noise source can be used to model the behavior of a decoherence-causing environment in neutron interferometers. With increasing noise amplitudes, Gaussian white noise causes an exponential loss of the interferometer contrast at both low and high interference order. The effect on the dynamical quantum phase was investigated, since the noise field was varied in one direction only. In the quasistatic regime, where the characteristic time scale of the noise is considerably longer than the time of flight of the neutron through the field region, analytic expressions have been obtained by averaging over the amplitude distribution of the noise field. Extension of the frequency bandwidth to higher frequencies leads to a weaker decay of contrast.

If noise fields are applied in both interferometer arms, the correlation of these two noise signals determines the contrast. For uncorrelated noise sources, the dephasing process is enforced. For two Gaussian white noise signals with the same frequency bandwidth, the decrease of contrast depends on the sum of their variances. On the other hand, application of synchronized identical noise signals leads to full recovery of the contrast. By insertion of an additional time delay between the two sources, the autocorrelation function of the signal is revealed.

At high interference order, a modulation in k space occurs that is related to the appearance of Schrödinger-cat-like states. As long as the energy transfer between the magnetic field and the neutron can be neglected, the dephasing effects on the modulated momentum distribution are comparable to the dephasing effects on the interference pattern at low interference order. The preparation of the Schrödinger-cat-like states becomes more difficult with increasing spatial separation but, within measurement accuracy, the loss of contrast is independent of the spatial separation.

Further experiments will deal with the energy exchange between the neutron and the magnetic noise field by use of time-resolved interferometry. The dependence of the dephasing process on different noise frequency bandwidths will be investigated in more detail as well.

ACKNOWLEDGMENTS

This work was supported by the doctoral program on complex quantum systems (COQUS) of the Austrian Science Foundation (FWF) and by the FWF Projects No. P-18943-N2D and No. P-20265. The authors want to thank K. Durstberger-Rennhofer and M. Suda for fruitful discussions on theoretical problems. Special thanks go to M. Baron, whose preliminary work on this subject strongly contributed to the success of these experiments.

[1] C. Davisson and L. H. Germer, Phys. Rev. **30**, 705 (1927).
[2] C. J. G. Möllenstedt, Z. Phys. **155**, 472 (1959).
[3] H. Rauch, W. Treimer, and U. Bonse, Phys. Lett. A **47**, 369 (1974).
[4] *Atom Interferometry,* edited by P. Berman (Academic Press, New York, 1997).
[5] M. Arndt, O. Nairz, J. Voss-Andreae, C. Keller, G. van der Zouw, and A. Zeilinger, Nature (London) **401**, 680 (1999).
[6] H.-P. Breuer and F. Petruccione, *The Theory of Open Quantum Systems* (Oxford University Press, Oxford, 2002).
[7] E. Joos, H. D. Zeh, C. Kiefer, D. Giulini, J. Kupsch, and I.-O. Stamatescu, *Decoherence and the Appearance of a Classical World in Quantum Theory* (Springer, Berlin, 2003).
[8] W. H. Zurek, Phys. Today **44**(10), 36 (1991).
[9] *Decoherence: Theoretical, Experimental, and Conceptual Problems*, edited by P. Blanchard, D. Giulini, E. Joos, C. Kiefer, and I.-O. Stamatescu, Lecture Notes in Physics 538 (Springer, Berlin, 2000).
[10] P. Sonnentag and F. Hasselbach, Phys. Rev. Lett. **98**, 200402 (2007).
[11] K. Hornberger, S. Uttenthaler, B. Brezger, L. Hackermüller, M. Arndt, and A. Zeilinger, Phys. Rev. Lett. **90**, 160401 (2003).
[12] L. Hackermuller, K. Hornberger, B. Brezger, A. Zeilinger, and M. Arndt, Nature (London) **427**, 711 (2004).
[13] A. Stern, Y. Aharonov, and Y. Imry, Phys. Rev. A **41**, 3436 (1990).
[14] J. Summhammer, K. A. Hamacher, H. Kaiser, H. Weinfurter, D. L. Jacobson, and S. A. Werner, Phys. Rev. Lett. **75**, 3206 (1995).
[15] J. Summhammer, Phys. Rev. A **47**, 556 (1993).
[16] R. A. Bertlmann, K. Durstberger, and Y. Hasegawa, Phys. Rev. A **73**, 022111 (2006).
[17] S. Filipp, J. Klepp, Y. Hasegawa, C. Plonka-Spehr, U. Schmidt, P. Geltenbort, and H. Rauch, Phys. Rev. Lett. **102**, 030404 (2009).
[18] D. F. Walls and G. J. Milburn, Phys. Rev. A **31**, 2403 (1985).
[19] D. L. Jacobson, S. A. Werner, and H. Rauch, Phys. Rev. A **49**, 3196 (1994).
[20] H. Rauch, Physica B **213-214**, 830 (1995).
[21] E. Sjöqvist, A. K. Pati, A. Ekert, J. S. Anandan, M. Ericsson, D. K. L. Oi, and V. Vedral, Phys. Rev. Lett. **85**, 2845 (2000).
[22] H. Rauch and S. Werner, *Neutron Interferometry* (Oxford University Press, Oxford, 2000).
[23] M. Baron, H. Rauch, and M. Suda, J. Opt. B: Quantum Semiclass. Opt. **5**, S241 (2003).
[24] M. Baron, Ph.D. thesis, TU Wien, Vienna, 2005.
[25] G. Lindblad, Commun. Math. Phys. **48**, 119 (1976).
[26] E. Wigner, Phys. Rev. **40**, 749 (1932).
[27] M. Suda, *Quantum Interferometry in Phase Space* (Springer, Berlin, 2006).
[28] H. Rauch, M. Suda, and S. Pascazio, Physica B **267**, 277 (1999).